Supporting Information

Hybrid organic-inorganic mononuclear Lanthanoid Single Ion Magnets.

Walter Cañón-Mancisidor*[a,b], Matias Zapata-Lizama[a,b], Patricio Hermosilla-Ibáñez[a,b], Carlos Cruz[b,c], Diego Venegas-Yazigi[a,b] and Guillermo Mínguez Espallargas*[d].

[a] Universidad de Santiago de Chile, Depto. de Química de los Materiales, Santiago, Chile.
E-mail: walter.canon@usach.cl.
[b] Center for the Development of Nanoscience and Nanotechnology, CEDENNA, Chile.
[c] Universidad Andres Bello, Facultad de Ciencias Exactas, Departamento de Ciencias Químicas, Chile.
[d] Instituto de Ciencia Molecular (ICMol), Universidad de Valencia, Valencia, Spain.
E-mail: guillermo.minguez@uv.es.

Index

1. Synthesis

All chemical reagents were directly used without further purification. $[NBu_4]_4[PW_{11}O_{39}H_3]$ was synthesized according to a previously reported method [1]. Hydrothermal synthesis was done using a Parr reactor of 23 ml model 4749.

1.1. Synthesis of $[NBu_4]_3[LnH(PW_{11}O_{39})(phen)_2]\cdot H_2O$.

The corresponding hydrated Ln^{III} acetates (0.1 mmol), $LnAc_3\cdot XH_2O$ where Ln^{III} = Dy^{III} (**LM^4-1-Dy**), Er^{III}(**LM^4-1-Er**) and Gd^{III} (**LM^4-1-Gd**) were mixed with $[NBu_4]_4[PW_{11}O_{39}H_3]$ (365 mg, 0.1 mmol) and phenanthroline (0.036 mg, 0.2 mmol) in 10 mL of water in a Parr reactor and heated under autogenous pressure at 160 °C for 48 hours. Under the same conditions, $DyAc_3\cdot XH_2O$ and $YAc_3\cdot XH_2O$ were mixed in Parr reactor in a ratio of 0.75 : 0.25 moles, giving compound (**LM^4-1-DyY**). The reaction mixture was filtered off, and pale pink crystals of **LM^4-1-Dy**, **LM^4-1-Er** and **LM^4-1-Gd**, suitable for X-ray diffraction, were obtained by mechanical separation. Then, these crystals were wash with water and acetone. Only microcrystalline material was obtained for **LM^4-1DyY**, but the different characterization techniques indicates that the compound is the same as for **LM^4-1-Dy**.

$[NBu_4]_3[DyH(PW_{11}O_{39})(phen)_2]\cdot H_2O$ (LM^4-1-Dy): FTIR ν (cm−1): 3548 (w), 2964 (m), 2878 (m), 1470 (m), 1382 (s), , 1077 (s), 1047 (w), 973 (m), 893 (s), 857 (s), 806 (s), 795 (s), 511 (s). Elem. Anal. for $Dy_1P_1W_{11}O_{40}C_{72}H_{127}N_7$; Teo. (Exp) C = 21,91%(21.76%), N = 2.48%(2.58%), H = 3.24%(3.33%). Elemental ratio estimated by electron probe microanalysis (EPMA): (Exp) Teo Dy : P : W = (1.07)1 : (0.95)1 : (10.96)11.

$[NBu_4]_3[ErH(PW_{11}O_{39})(phen)_2]\cdot H_2O$ (LM^4-1-Er): FTIR ν (cm−1): 3544 (w), 2961 (m), 2934(m), 1458 (m), 1377 (s), , 1078 (s), 973 (m), 884 (s), 794 (s), 592 (s), 666 (s), 521 (s). Elem. Anal. for $Er_1P_1W_{11}O_{40}C_{72}H_{127}N_7$; Teo. (Exp) C = 21,89%(21.96%), N = 2.48%(2.34%), H = 3.24%(3.15%). Elemental ratio estimated by electron probe microanalysis (EPMA): (Exp) Teo Er : P : W = (0.98)1 : (0.97)1 : (11.03)11.

$[NBu_4]_3[GdH(PW_{11}O_{39})(phen)_2]\cdot H_2O$ (LM^4-1-Gd): FTIR ν (cm−1): 3547 (w), 2965 (m), 2925 (m), 2870 (m), 1463 (m), 1378(w), 1064 (s), 972 (s), 888 (w), 796 (s), 612 (s), 505 (s). Elem. Anal. for $gd_1P_1W_{11}O_{40}C_{72}H_{127}N_7$; Teo. (Exp) C = 21,94%(21.88%), N = 2.49%(2.51%), H = 3.25%(3.29%). Elemental ratio estimated by electron probe microanalysis (EPMA): (Exp) Teo Gd : P : W = (0.97)1 : (1.02)1 : (11.03)11.

$[NBu_4]_3[Dy_{0.25}Y_{0.75}H(PW_{11}O_{39})(phen)_2]\cdot H_2O$ (LM^4-1-DyY): FTIR ν (cm−1): 3553 (w), 2955 (m), 2922 (m), 2870 (m), 1461 (m), 1073 (s), 972 (s), 891 (w), 796 (s), 684 (s), 503 (s). Elem. Anal. for $Dy_{0.25}\,Y_{0.75}P_1W_{11}O_{40}C_{72}H_{127}N_7$; Teo. (Exp) C = 22.22%(21.98%), N = 2.52%(2.45%), H = 3.29%(3.34%). Elemental ratio estimated by electron probe microanalysis (EPMA): (Exp) Teo Dy : Y : P : W = (0.26)0.25 : (0.77)0.75 : (1.05)1 : (10.98)11.

1.2. Physical Measurements

FTIR-ATR (Fourier Transform Infrared- Attenuated Total Reflectance) spectra (4000–400 cm^{-1}) of the compounds were measured using a Jasco FTIR-4600 spectrophotometer equipped with an ATR PRO ONE (Jasco, Easton, MD, USA), Figure S1. Elemental analyses (C, N, H) of bulk samples were performed using a Thermo elemental analyser Flash 2000. The Ln : P : W ratios of the bulk samples were estimated by electron probe microanalysis (EPMA) performed with a Jeol, JSM 5410 equipped with an EDAX NORAN microprobe, Table S1.

1.2.1. Fourier transform infrared spectroscopy (FTIR)

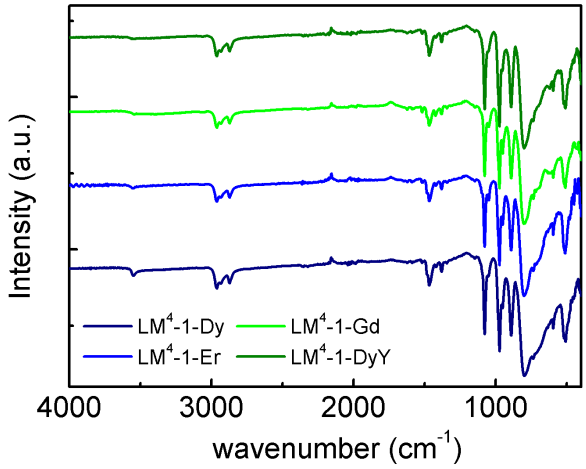

Figure S1. Infrared Spectra of compounds $[NBu_4]_3[Ln(HPW_{11}O_{39})(phen)_2]\cdot H_2O$, where where Ln^{III} = Dy^{III} (**LM^4-1-Dy**), Er^{III}(**LM^4-1-Er**), Gd^{III} (**LM^4-1-Gd**) and $Dy^{III}_{0.25}Y^{III}_{0.75}$ (**LM^4-1-DyY**).

1.2.2. Electron Probe Microanalysis

Table S1. Atomic relation obtained of tungsten, phosphorous and lanthanide by electron probe microanalysis for the crystalline materials of compounds $[NBu_4]_3[LnH(PW_{11}O_{39})(phen)_2]\cdot H_2O$, where where Ln^{III} = Dy^{III} (**LM^4-1-Dy**), Er^{III}(**LM^4-1-Er**), Gd^{III} (**LM^4-1-Gd**) and $Dy^{III}_{0.25}Y^{III}_{0.75}$ (**LM^4-1-DyY**). In parenthesis expected value.

Compound	Tungsten	Phosphorous	Lanthanide	Yttrium
LM^4-1-Dy	10.96 (11)	0.95 (1)	1.07 (1)	-
LM^4-1-Er	11.03 (11)	0.97 (1)	0.98 (1)	-
LM^4-1-Gd	11.03 (11)	1.02 (1)	0.97 (1)	-
LM^4-1-DyY	10.98 (11)	1.05 (1)	0.77 (0.75)	0.26 (0.25)

2. *X-Ray Diffraction*

2.1. Single Crystal X-Ray Diffraction

A single crystal for each compound was taken directly from the synthesis vessel and examined under microscope, suggesting acceptable quality. It was then mounted on the tip of a glass fibre. The intensities for **LM^4-1-Dy**, **LM^4-1-Er** and **LM^4-1-Gd** were recorded on a Bruker Smart Apex diffractometer, using separations of 0.3° between frames and 10s by frame. Data sets were reduced by using SAINTPLUS [2], while the structure was solved by direct methods and completed by Difference Fourier Synthesis. Least-squares refinement was conducted by using SHELXL [3,4]. All atoms were anisotropically refined, whereas the N and C atoms of the tetra-n-butylammonium cations where isotropically refined. Hydrogen atom positions were calculated after each cycle of refinement with SHELXL using a riding model for each structure, with a C–H distance of 0.93 Å or 0.97 Å. U_{iso}(H) values were set equal to 1.2U_{eq} of the parent carbon atom. Additional crystallographic and refinement details are given in Table X. Structural drawings were carried out with DIAMOND-3.2k, supplied by Crystal Impact [5]. Crystallographic data for the structure reported in this paper have been deposited with the Cambridge Crystallographic Data Centre as supplementary publication number CCDC-1951515 for **LM^4-1-Dy**, CCDC-1951516 for **LM^4-1-Er** and CCDC-1951519 for **LM^4-1-Gd**. Copies of the data can be obtained free of charge via http://www.ccdc.cam.ac.uk/conts/retrieving.html, or from the Cambridge Crystallographic Data Centre, 12 Union Road, Cambridge CB2 1EZ, UK; fax: (+44) 1223-336-033; or e-mail: deposit@ccdc.cam.ac.uk.

Table S2. Crystallography data and structure refinement for $[NBu_4]_3[LnH(PW_{11}O_{39})(phen)_2]\cdot H_2O$, where Ln^{III} = Dy^{III} (**LM^4-1-Dy**), Er^{III}(**LM^4-1-Er**) and Gd^{III} (**LM^4-1-Gd**).

Complex	**LM^4-1-Dy**	**LM^4-1-Er**	**LM^4-1-Gd**
CCDC	1951515	1951516	1951519
Formula weight	3946.51	3951.27	3941.26
Temperature/K	150(2)	297(2)	297(2)
Crystal system	Monoclinic	Monoclinic	Monoclinic
Space group	*P2$_1$/c*	*P2$_1$/c*	*P2$_1$/c*
a/Å	22.9224(15)	23.510(3)	23.6346(19)
b/Å	15.4103(10)	15.593(2)	15.5653(13)
c/Å	28.4878(19)	28.591(4)	28.567(2)
β/°	96.4140(10)	97.187(2)	97.2100(10)
Volume/Å^3	10000.1(11)	10399(3)	10426.1(15)
Z	4	4	4
ρ_{calc}g/cm^3	2.621	2.522	2.509
μ/mm^{-1}	13.430	13.003	12.801
F(000)	7288.0	7288.0	7272.0
Crystal size/mm^3	0.21 × 0.13 × 0.08	0.26 × 0.15 × 0.07	0.19 × 0.12 × 0.08
2Θ range for data collection/°	3.19 to 55.982°	2.98 to 52°	2.986 to 55.968°
Index ranges	-30 ≤ h ≤ 30, -20 ≤ k ≤ 20, -37 ≤ l ≤ 37	-27 ≤ h ≤ 28, -19 ≤ k ≤ 19, -35 ≤ l ≤ 35	-31 ≤ h ≤ 31, -20 ≤ k ≤ 20, -37 ≤ l ≤ 37
Reflections collected	82543	78389	86733
Independent reflections	22426[R(int) = 0.0692]	20435[R(int) = 0.1221]	25140[R(int) = 0.0870]
Data/restraints/parameters	22426/57/919	20435/173/907	25140/133/907
Goodness-of-fit on F^2	1.024	1.001	1.014
Final R indexes [I>=2σ (I)]	R_1 = 0.0532, wR_2 = 0.1244	R_1 = 0.0718, wR_2 = 0.1829	R_1 = 0.0696, wR_2 = 0.1748
Final R indexes [all data]	R_1 = 0.0918, wR_2 = 0.1413	R_1 = 0.1482, wR_2 = 0.2309	R_1 = 0.1357, wR_2 = 0.2150

2.2. Structural Analysis

It is possible to mention that hybrid inorganic-organic systems are usually obtained forming dinuclear compounds, as has been reported in the literature[6,7] and also only one dinuclear inorganic-organic hybrid system presents a N-containing organic ligand has been reported in the literature by Xiao et al.[8]. However, no mononuclear hybrid inorganic-organic systems have been reported in the literature, being the complexes presented in this work, the first example of mononuclear lanthanoid complexes with a lacunary polyoxometalate and a N-containing organic ligand, opening the possibility to obtain a completely new family of mononuclear compounds varying the nature of the aromatic N-organic ligand (Figure S2).

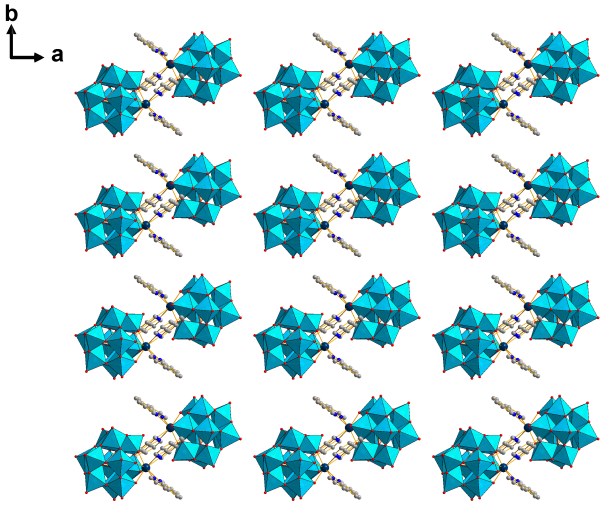

Figure S2. View along the *c*-axis of the crystalline packing of hybrid organic-inorganic complexes $[Ln(HPW_{11}O_{39})(phen)_2]^{3-}$. Hydrogen atoms, water molecule and $[n\text{-}NBu^4]^+$ ions have been omitted for clarity. Hydrogen atoms, water molecule and $[n\text{-}NBu_4]^+$ ions are omitted for clarity. Colour label: Ln (dark blue), W (cyan), N (blue), C (grey) O (red) and P (light yellow).

The metal-metal distances between the closest lanthanoids, centres are 9.714(1) Å, 9.783(2) Å and 9.778(1) Å, for **LM^4-1-Dy**, **LM^4-1-Er** and **LM^4-1-Gd** complexes, respectively. The crystal lattice of these compounds are also stabilized by the existence of π- π stacking between the aromatic rings (N20 C17 C18 C19 C23 C24 ; N40 C37 C38 C39 C43 C44) of the phenanthroline ligands, with distances of 3.482 Å, 3.568 Å and 3.556 Å, for **LM^4-1-Dy**, **LM^4-1-Er** and **LM^4-1-Gd** complexes (Figure S3) and also by the existence of hydrogen bonds in the system.

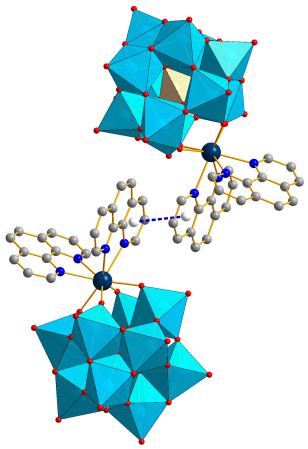

Figure S3. π- π stacking between the aromatic rings of the phenanthroline ligands. Hydrogen atoms, water molecule and $[n\text{-}NBu_4]^+$ ions are omitted for clarity. Colour label: Ln (dark blue), W (cyan), N (blue), C (grey) O (red) and P (light yellow).

Table S3. Selected bond distances (Å) for $[LnH(PW_{11}O_{39})(phen)_2]^{4-}$, where Ln^{III} = Dy^{III} (**LM^4-1-Dy**), Er^{III}(**LM^4-1-Er**) and Gd^{III} (**LM^4-1-Gd**).

Ln^{III}	N11	N20	N31	N40	O7	O9	O10	O12
Dy^{III}	2.597(9)	2.559(10)	2.549(10)	2.604(10)	2.325(9)	2.259(8)	2.283(8)	2.328(8)
Er^{III}	2.608(19)	2.559(17)	2.550(2)	2.618(18)	2.330(14)	2.225(14)	2.309(13)	2.307(14)
Gd^{III}	2.646(15)	2.590(14)	2.615(18)	2.646(16)	2.356(12)	2.277(11)	2.309(11)	2.358(11)

Table S4. Bond Valence Sum[9] (BVS) values for the **LM^4-1-Dy** of the oxygen atoms of the $[PW_{11}O_{39}]^{7-}$ anion, in order to determine the location of the proton[10].

$[PW_{11}O_{39}]^{7-}$	**BVS**	$[PW_{11}O_{39}]^{7-}$	**BVS**	$[PW_{11}O_{39}]^{7-}$	**BVS**
O1	2.08	O14	1.74	O27	1.94
O2	1.96	O15	1.93	O28	1.88
O3	2.03	O16	2.01	O29	1.99
O4	1.76	O17	1.99	O30	2.06
O5	1.86	O18	1.81	O31	1.78
O6	1.96	O19	2.01	O32	1.80
O7	1.48	O20	2.10	O33	1.77
O8	2.04	O21	2.00	O34	1.99
O9	1.90	O22	2.02	O35	1.79
O10	1.73	O23	2.05	O36	2.05
O11	2.03	O24	1.93	O37	1.80
O12	1.72	O25	2.09	O38	1.82
O13	2.01	O26	1.97	O39	1.82

2.3. *Powder Crystal X-Ray Diffraction*

Crystalline and microcrystalline samples of all compounds were slightly grounded with a pestle in an agate mortar and filled into 0.5 mm borosilicate capillaries prior to being mounted and aligned on an Empyrean PANalytical powder diffractometer, using Cu Kα radiation (λ = 1.54056 Å). For each sample, two or three repeated measurements were collected at room temperature (2θ = 2 – 40°) and merged into a single diffractogram.

XRPD analysis of complexes were done to the crystalline and microcrystalline material after been washed with several portions of acetone. The XRPD pattern of $[NBu_4]_3[LnH(PW_{11}O_{39})(phen)_2]\cdot H_2O$ is quite similar for all the Ln complexes, but some differences exist that are due to the existence of amorphous material. The crystalline products of $[NBu_4]_3[Ln(HPW_{11}O_{39})(phen)_2]\cdot H_2O$, where Ln = Dy^{III} (**LM^4-1-Dy**), Er^{III} (**LM^4-1-Er**), Gd^{III} (**LM^4-1-Gd**) and $Dy^{III}_{0.25}Y^{III}_{0.75}$ (**LM^4-1-DyY**) are isostructural and also are in agreement with their simulated patterns, which demonstrates that the crystal structures of the compounds are truly representative of the bulk materials. The differences in intensity are due to the preferred orientation of the powder samples (Figures S4 and S5).

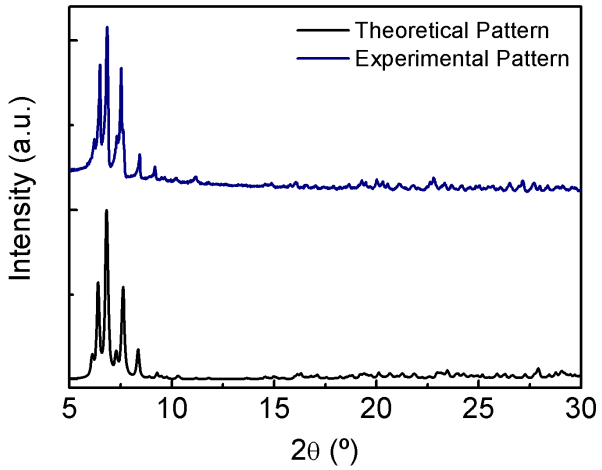

Figure S4. PXRD patterns of the crystalline phase of compound, $[NBu_4]_3[DyH(PW_{11}O_{39})(phen)_2]\cdot H_2O$ (**LM^4-1-Dy**), in black, and the theoretical pattern of compounds **LM^4-1-Dy**.

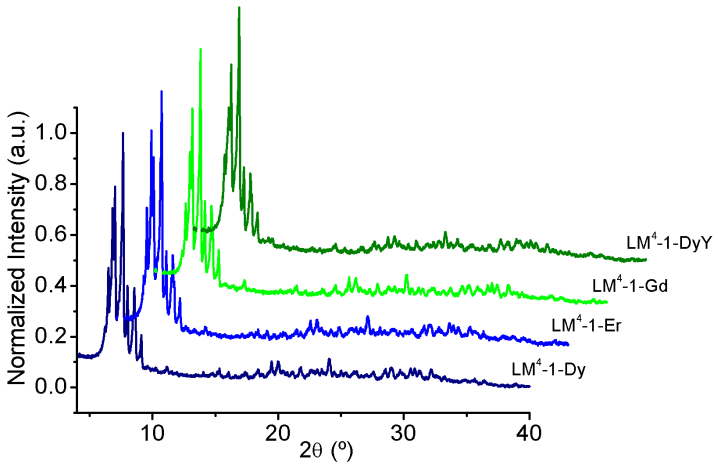

Figure S5. PXRD patterns of the different crystalline phases of the compounds $[NBu_4]_3[LnH(PW_{11}O_{39})(phen)_2]\cdot H_2O$, where where Ln^{III} = Dy^{III} (**LM^4-1-Dy**), Er^{III}(**LM^4-1-Er**), Gd^{III} (**LM^4-1-Gd**) and $Dy^{III}_{0.25}Y^{III}_{0.75}$ (**LM^4-1-DyY**).

2.4. SHAPE analysis

In order to describe the geometry of the Ln complexes of this work, continuous shape measurement (CShM´s) calculations were done using the SHAPE code [11,12]. This code compare how distorted is the octacoordinated lanthanoid ion compare to other octacoordinated ideal geometries and calculate a value indicating how distorted is the centre compared to the eleven possibilities that an octacoordinated system can have. The calculations show that the geometry of the Ln complexes can be described as a square antiprism (sa), which means that the Ln centres present a psedo-D_{4d} symmetry. The geometry that these systems present is not unusual since most octacoordinated lanthanoid complexes present distorted forms of square antiprism, triangular dodecahedron or bicapped trigonal prism geometries[13–17] (Figure S6 and S7).

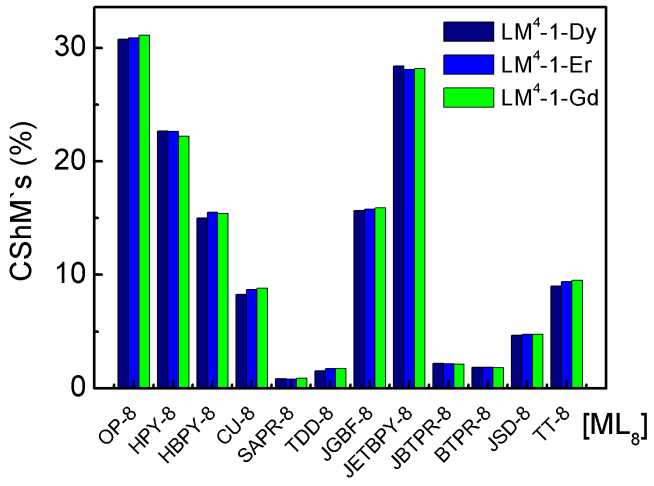

Figure S6. Results of the SHAPE measurements for the $[LnH(PW_{11}O_{39})(phen)_2]^{4-}$ complexes, where for Ln = Dy^{III} (**LM^4-1-Dy**), Er^{III} (**LM^4-1-Er**) and Gd^{III} (**LM^4-1-Gd**).

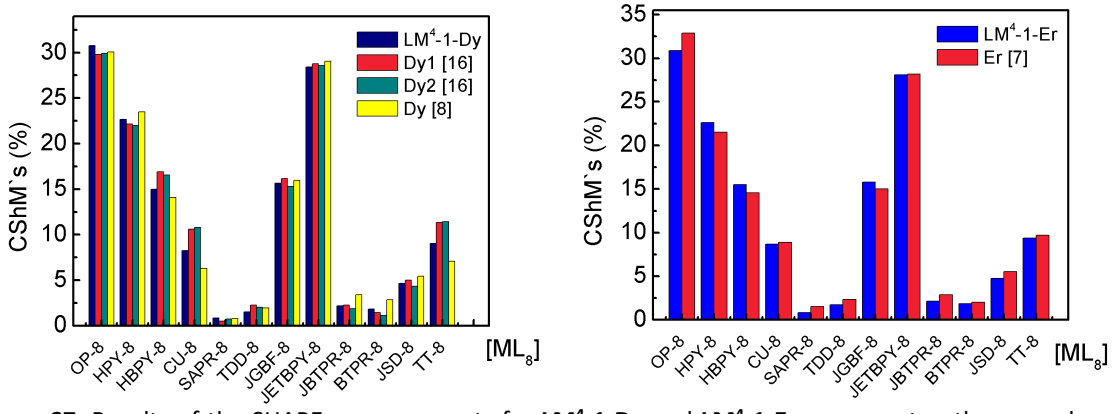

Figure S7. Results of the SHAPE measurements for **LM^4-1-Dy** and **LM^4-1-Er** compare to other complexes form by inorganic or hybrid organic-inorganic ligand[7,8,18]. In parenthesis the associated references for the comparison.

3. Magnetic Susceptibility Measurements

3.1. Static Magnetic Susceptibility

Magnetic measurements were performed on ground crystals of the different compounds in a Quantum Design Physical Property Measurement System (PPMS) and in a PPMS DynaCoolTM (Quantum Design). Variable-temperature (2 - 300 K) direct current (dc) magnetic susceptibility measurements were carried out under an applied field of 1 kG, and variable field magnetization measurements up to 5 T were performed at 2.0 K for all compounds. The susceptibility data were corrected for the diamagnetic contributions of the sample, using Pascal´s constants[19]. Variable-temperature (2 - 12 K) alternating current (ac) magnetic susceptibility measurements using an oscillating field between 1 to 7 G, at frequencies in the range of 10 – 10000 Hz were carried out under a zero-dc field for **LM^4-1-Dy**. The same measurement was repeated under an optimal dc field of 2 kG. For **LM^4-1-Er**, variable-temperature (2 - 10 K) alternating current (ac) magnetic susceptibility measurements using an oscillating field between 1 to 7 G, at a single frequency of 2000 Hz were carried out under 0, 1 kG, 2 kG and 3 kG dc field. The same measurement was repeated under a dc field of 1 kG.

Magnetic dc susceptibility measurements were carried out between 2 and 300 K at 1 kG for complexes **LM^4-1-Ln**, **Ln = Dy, Er**, and **DyY** (Figure 2). The susceptibility values of all the complexes are in good agreement with the expected values for mononuclear complexes; Dy^{III} (S = 5/2, L =5, $^6H_{15/2}$, g = 4/3, χT = 14.17 emu K mol^{-1}), Er^{III} (S = 3/2, L =6, $^4I_{15/2}$, g = 36/5, χT = 11.48 emu K mol^{-1}) and Gd^{III} (S =7/2, L =0, $^8S_{7/2}$, g = 2, χT = 7.88 emu K mol^{-1}) [20,21]. For **LM^4-1-Gd**, the susceptibility measurement shows that the system is paramagnetic, so the χT values decrease at low temperatures is due to the thermal depopulation of the Stark sublevels[22]. For **LM^4-Dy** and **LM^4-1-DyY**, it is possible to observed that the magnetic response is the same at high temperatures, and only at low temperature the susceptibility is higher for second complex. Magnetization measurements were done for all the compounds at 2K between 0 to -90 kG and for **LM^4-1-Dy**, **LM^4-1-Er** and **LM^4-1-DyY** compounds the magnetization does not saturate even at high fields. On the other hand, for **LM^4-1-Gd** the magnetization reaches a value of 6.95 Nβ, which is almost the expected value of 7 electrons**,** suggesting that paramagnetic behavior is predominant at 2 K (Figure S8). The reduced magnetization data for compounds **LM^4-1-Dy** and

LM^4-1-Er were collected between 0 to 90 kG at 2, 3 and 5 K, and the non-superposition of the iso-field lines shows the anisotropic character of the system (Figure S9). These results suggest that the Dy^{III} and Er^{III} compounds could have dynamic response the magnetization measurements (hysteresis loop) were done for compounds **LM^4-1-Dy** and **LM^4-1-Er**, at 2K between -90 to 90 kG. Only the dysprosium complex presents a butterfly magnetic hysteresis suggesting the presence of slow magnetic relaxation and Quantum Tunnelling of Magnetization (QTM), as also observed for other lanthanoid SIMs[20] (Figure S10).

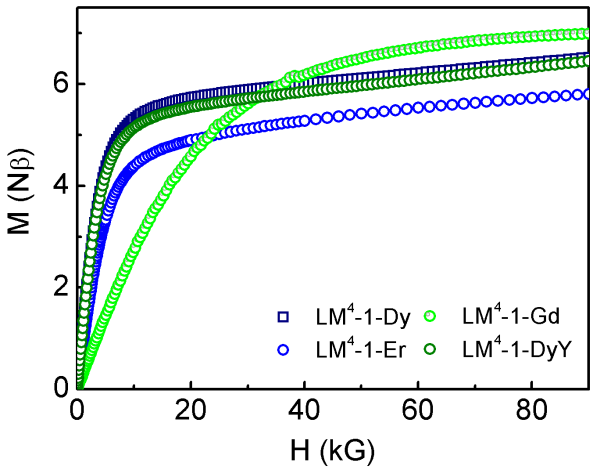

Figure S8. Magnetization measurements at 2K for compounds **LM^4-1-Dy**, **LM^4-1-Er**, **LM^4-1-Gd** and **LM^4-1-DyY.**

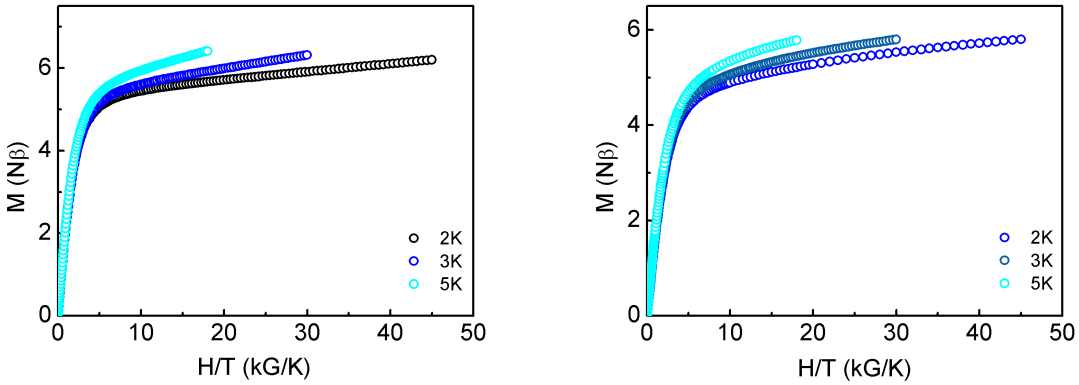

Figure S9. Reduced magnetization vs H/T measurements at 2, 3 and 5 K for **LM^4-1-Dy** and **LM^4-1-Er**.

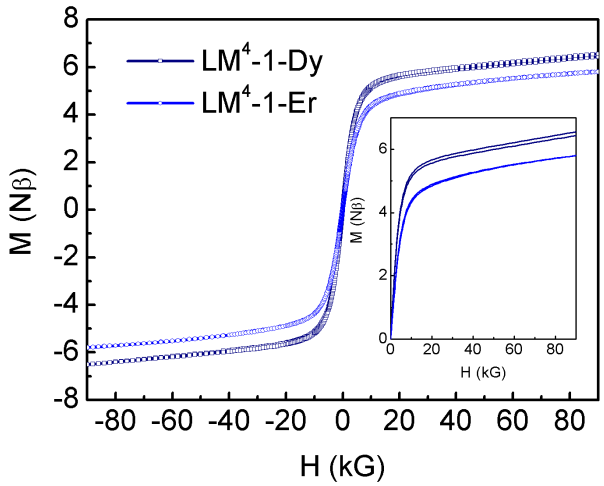

Figure S10. M(H) measurements between -90 kG to 90 kG for the complexes **LM^4-1-Dy** and **LM^4-1-Er**. Inset: M(H) of the dysprosium complexes showing the existence of hysteresis in these complexes.

3.2. Dynamic Magnetic Susceptibility

For **LM^4-1-Dy** in the absence of an external dc field, dynamic magnetic measurements (ac) present an out-of-phase signal (χ''), which is frequency-dependent, although no maxima are observed (Figure S11). This behaviour could be due to the existence of fast relaxation of the magnetization through a quantum tunnelling mechanism. This phenomenon can be quenched by the application of an external dc field that drives the magnetic levels away from the hyperfine avoided crossing region[23–26]. The dynamic magnetic measurement was done at an optimal field of 2 kG, as is shown in the supporting information (Figure S12). In the ac-susceptibility versus frequencies measurements a single maximum is observed related to the relaxation process of this system (Figure S13).

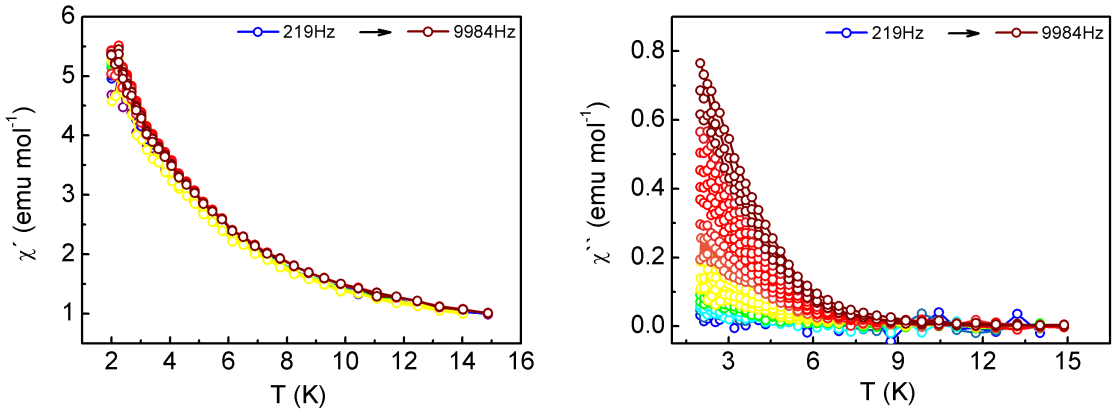

Figure S11. ac susceptibility measurement at zero-dc field at different frequencies for **LM^4-1-Dy**.

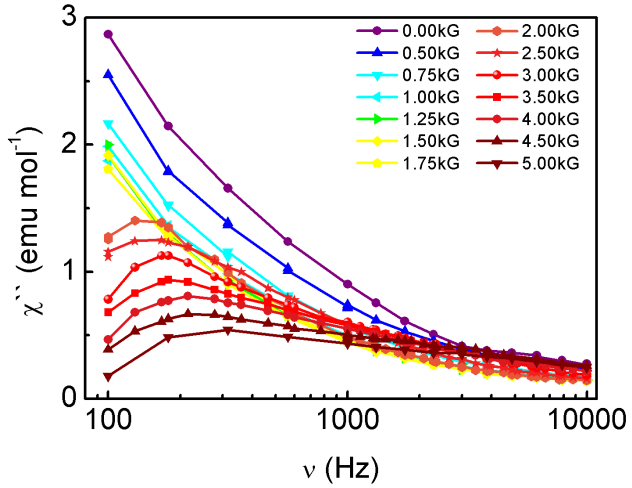

Figure S12. ac susceptibility χ´´(ν) measurement at T = 3K for **LM^4-1-Dy** at different dc fields at 2K temperatures to obtain the optimal field.

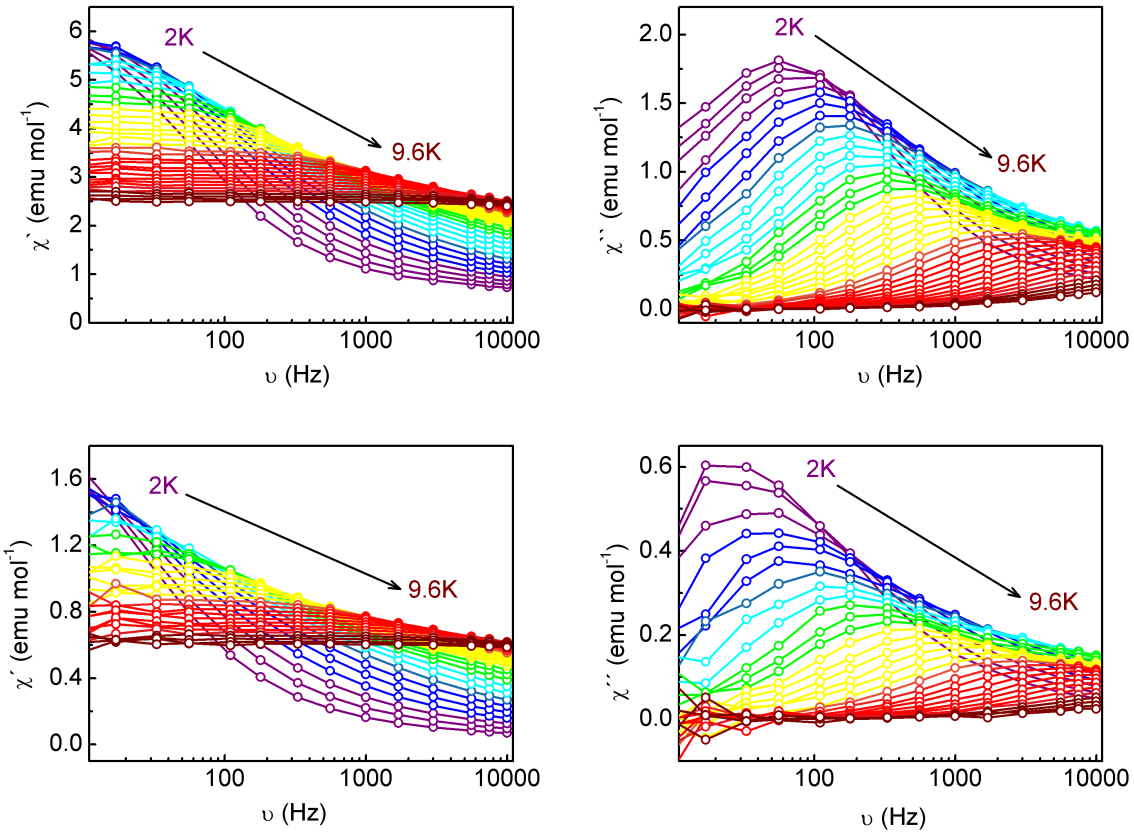

Figure S13. out-phase and in-phase susceptibility measurements for **LM^4-1-Dy** $[DyH(PW_{11}O_{39})(phen)_2]^{3-}$ and for **LM^4-1-DyY** $[Dy_{0.25}Y_{0.75}H(PW_{11}O_{39})(phen)_2]^{3-}$ between 2K to 9.6K at an optimal field of 2 kG.

Table S5. Summarized values of the SHAPE values and relaxation dynamics parameters of the Orbach mechanism for compounds **LM^4-1-Dy**, **[Dy(PW$_{11}$O$_{39}$)$_2$]$^{11-}$**, **[Dy(Pc)$_2$]$^-$** and **[Dy(acac)$_3$(phen)]**.
Pc = phthalocyanine; acac = acetylacetonate; phen = phenanthroline

Compound	CShM`s (%)	τ_0 (s)	U_{eff} (cm^{-1})
LM^4-1-Dy	0.858	5.32 x 10^{-9}	36.4
[18] **[Dy(PW$_{11}$O$_{39}$)$_2$]$^{11-}$**	0.768	9.60 x 10^{-12}	36.3
[27] **[Dy(Pc)$_2$]$^-$**	0.580	6.25 x 10^{-6}	28.0
[28] **[Dy(acac)$_3$(phen)]**	0.425	5.73 x 10^{-6}	42.1

In order to explain the relaxation process of Single Ion Magnets, the relaxation mechanisms such as QTM and spin–lattice developed for paramagnetic metal salts, can be also applied to this kind of systems. According to these studies three main relaxation mechanisms can be defined, that arise from the energy exchange between the paramagnetic centres and the phonon radiations; Direct, Raman and Orbach [29]. Also, there is one relaxation mechanism that does not depend on the temperature of the system. This phenomenon is caused by the existence of transverse anisotropy induced by the distortion from the axial symmetry, which is referred as Quantum Tunnelling of Magnetization (QTM) [30]. Furthermore, a quantitative formulation of relaxation times τ for the four relaxation processes according to the above theory is usually applied in SMM field to model the magnetic data (equation 1 in main text) [30–39]. In order to study the relaxation mechanism of **LM^4-1-Dy** at the optimal dc field, the equation presented above have been used by several authors in order to describe properly the relaxation dynamics of these magnetic systems [30–39].

Cole-Cole plots for **LM^4-1-Dy** were used to extrapolate the alpha value (Figure S14). The distribution of the relaxation times can be studied by plotting χ'' versus χ' in an Argand plot. The fit of the data to a general Debye model[40] (equation S1) results in adequate description of the experimental points. At low temperatures, the α value is around 0.3, suggesting that multiple relaxation mechanism are present like direct, Raman, QTM at low temperatures. When increasing the temperature, the α value decrease to 0.2 to 0.1 inferring that the Orbach mechanism becomes dominant at higher temperatures (Figure S15 and table S4).

$$\chi''(\chi') = \frac{\chi_T - \chi_S}{2\tan\left[\frac{1}{2}\pi(1-\alpha)\right]}\left[\left(\frac{\chi_T - \chi_S}{2}\right)^2 - \left(\frac{\chi_T - \chi_S}{2\tan\left[\frac{1}{2}\pi(1-\alpha)\right]}\right)^2 - \left(\chi' - \frac{\chi_T + \chi_S}{2}\right)^2\right]^{\frac{1}{2}} \qquad \text{(S1)}$$

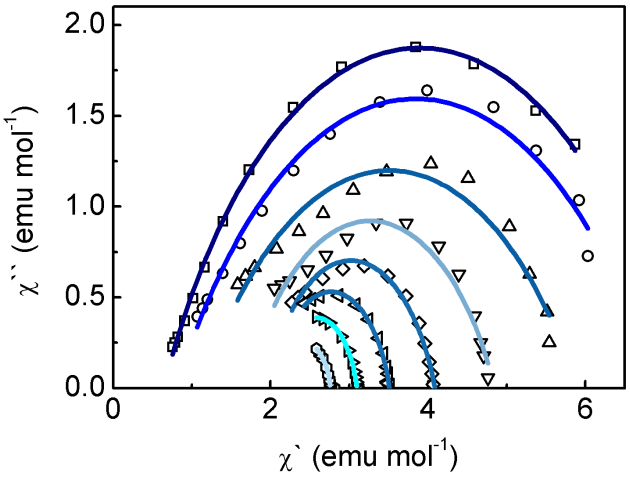

Figure S14. Argand plots at different temperatures, T = 2 (dark blue) to 9 (cyan) K, for compound **LM^4-1-Dy**. Solid lines in the Cole–Cole plots are fitting results from one Debye functions.

Table S6. Obtained values of χ_T, χ_S and α of the Argand plots by the Debye model at 2000G for **LM^4-1-Dy**.

T (K)	χ_T	χ_S	α
2	7.52	0.25	0.30
3	7.38	0.30	0.34
4	6.35	0.67	0.35
5	5.03	1.49	0.30
6	4.16	1.88	0.24
7	3.54	1.99	0.20
8	3.11	2.06	0.16
9	2.76	2.16	0.12

Moreover, compound **LM^4-1-Er** presents frequency dependent signals only when a dc field is applied, making this Erbium compound a field induced Single Ion Magnet (SIMs), being these systems scarce compared to the Dy^{III} ones[35,41–43]. However, the QTM phenomenon in this system cannot be suppress even when applying different dc fields since no maxima can be observed. (Figure S16 and S17) [44]. In order to study the dynamic magnetic relaxation of this compound, an approach to the Arrhenius equation (equation S2) was used in order to study the relaxation dynamics [45–47].

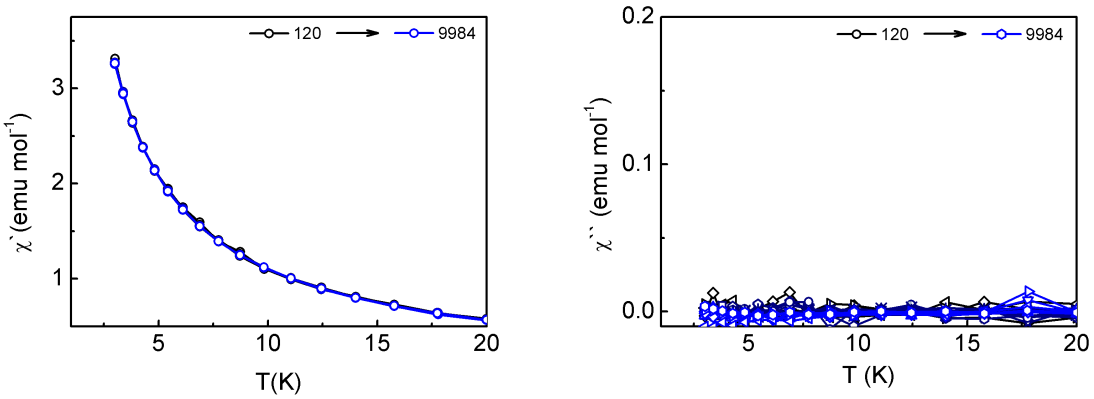

Figure S15. ac susceptibility measurement at different temperatures (χ´(T) and χ´´(T)) of **LM^4-1-Er** at zero dc fields at different frequencies.

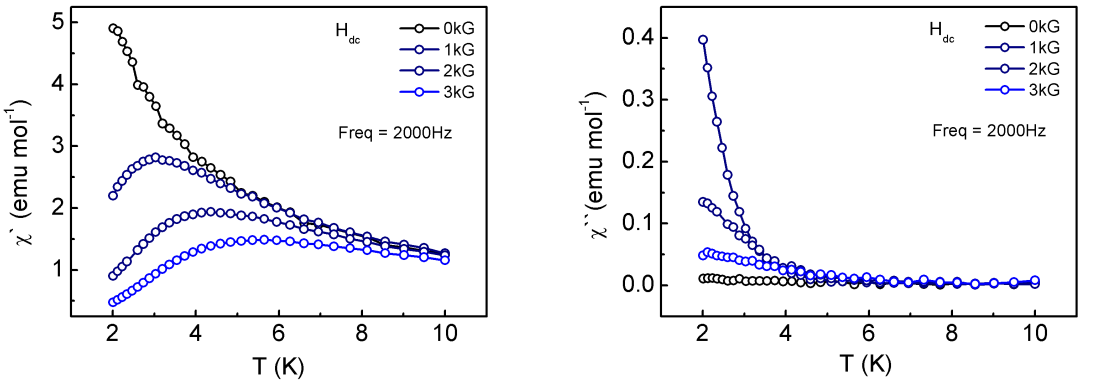

Figure S16. ac susceptibility measurement at different temperatures (χ´(T) and χ´´(T)) of **LM^4-1-Er** at different dc fields at ν = 2000 Hz to obtain the optimal field.

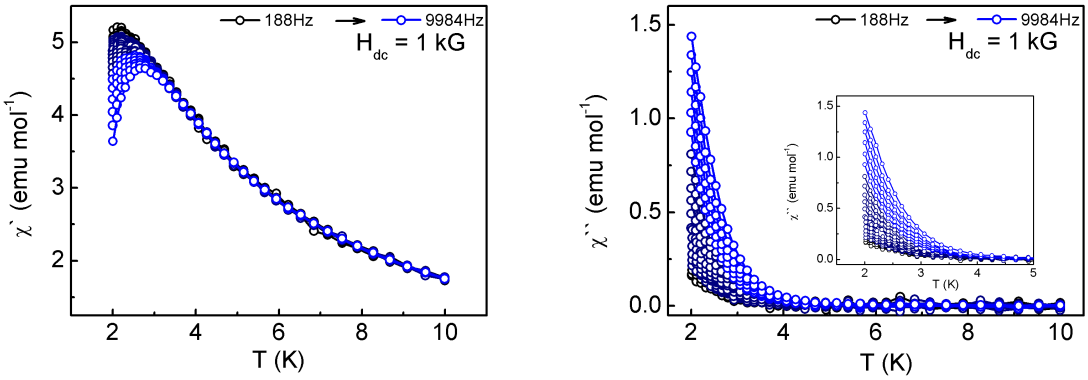

Figure S17. ac susceptibility measurements (in-phase and out-phase) obtained in the PPMS, at H_{dc} = 1 kG for $[NBu_4]_3[ErH(PW_{11}O_{39})(phen)_2]\cdot H_2O$ (**LM^4-1-Er**).

$$Ln\left(\frac{\chi^{''}}{\chi^{'}}\right) = Ln(\omega\tau_0) + \frac{U_{eff}}{k_B T} \qquad \text{(S2)}$$

By using this approach, we performed a fit of these data at different frequencies under a dc field of 1 kG. A good fit was achieved with energies barriers of the relaxations of the magnetization (U_{eff}) of 7.67 cm^{-1} (4328 Hz); 7.68 cm^{-1} (5339 Hz); 7.61 cm^{-1} (6582 Hz); 7.46 cm^{-1} (8117 Hz) and 7.25 cm^{-1} (9984 Hz), being the average U_{eff} = 7.53 (0.18) cm^{-1} and an average τ_0 = 3.52 (0.67) x 10^{-6} s^{-1} see Figure S17 and Table 1.

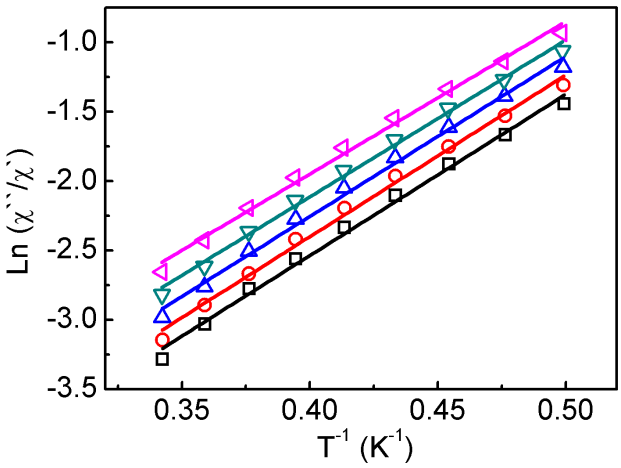

Figure S18. Relaxation times versus temperature using Arrhenius plot for compound **LM^4-1-Er**. Colour labels of the frequencies: 4328 Hz (black); 5339 Hz (red); 6582 Hz (blue); 8117 Hz (cyan) and 9984 Hz (Black).

Table S7. Summarized values of the relaxation dynamics for compounds **LM^4-1-Dy**, **LM^4-1-DyY** and **LM^4-1-Er**. [a]Fitting parameters were obtained with equation 1. [b]Fitting parameters are obtained with equation S2.

Compound	C ($K^{-n}s^{-1}$)	n	τ_{QTM} (s)	τ_0 (s)	U_{eff} (cm^{-1})
LM^4-1-Dy [a]	0.997	3.65	0.021	5.32 x 10^{-9}	36.4
LM^4-1-DyY [a]	0.206	4.61	0.043	5.21 x 10^{-9}	36.3
LM^4-1-Er [b]	-	-	-	3.52 x 10^{-6}	7.53

4. References

1 E. Radkov and R. H. Beer, *Polyhedron*, 1995, **14**, 2139–2143.
2 SAINTPLUS, 1999, Version 6.02; Brucker AXS: Madison, WI, USA.
3 G. M. Sheldrick, *Acta Crystallogr. Sect. C Struct. Chem.*, 2015, **71**, 3–8.
4 G. M. Sheldrick, *Acta Crystallogr. Sect. A Found. Adv.*, 2015, **71**, 3–8.
5 K. Brandenburg, *Diamond, Version 3.2k, Cryst. Impact GbR, Bonn, Ger.*, 2014.
6 D. Zhang, C. Zhang, H. Chen, P. Ma, J. Wang and J. Niu, *Inorganica Chim. Acta*, 2012, **391**, 218–223.
7 J. Niu, K. Wang, H. Chen, J. Zhao, P. Ma, J. Wang, M. Li, Y. Bai and D. Dang, *Cryst. Growth Des.*, 2009, **9**, 4362–4372.
8 L. Xiao, T.-T. Zhang, Z. Liu, X. Shi, H. Zhang, L. Yin, L.-Y. Yao, C.-C. Xing and X.-B. Cui, *Inorg. Chem. Commun.*, 2018, **95**, 86–89.

9 I. D. Brown and D. Altermatt, *Acta Crystallogr. Sect. B Struct. Sci.*, 1985, **41**, 244–247.
10 D. Zhang, Y. Zhang, J. Zhao, P. Ma, J. Wang and J. Niu, *Eur. J. Inorg. Chem.*, 2013, **2013**, 1672–1680.
11 D. Casanova, J. Cirera, M. Llunell, P. Alemany, D. Avnir and S. Alvarez, *J. Am. Chem. Soc.*, 2004, **126**, 1755–1763.
12 D. Casanova, M. Llunell, P. Alemany and S. Álvarez, *Chem. - A Eur. J.*, 2005, **11**, 1479–1494.
13 F. J. Kettles, V. A. Milway, F. Tuna, R. Valiente, L. H. Thomas, W. Wernsdorfer, S. T. Ochsenbein and M. Murrie, *Inorg. Chem.*, 2014, **53**, 8970–8978.
14 J. Zhu, C. Wang, F. Luan, T. Liu, P. Yan and G. Li, *Inorg. Chem.*, 2014, **53**, 8895–8901.
15 M. M. Hänninen, A. J. Mota, D. Aravena, E. Ruiz, R. Sillanpää, A. Camón, M. Evangelisti and E. Colacio, *Chem. - A Eur. J.*, 2014, **20**, 8410–8420.
16 X. Li, D. Y. Wei, S. J. Huang and Y. Q. Zheng, *J. Solid State Chem.*, 2009, **182**, 95–101.
17 X. Q. Zhang, M. S. Lin, B. Hu, W. Q. Chen, L. N. Zheng, J. Wu, Y. M. Chen, F. Y. Zhou, Y. H. Li and W. Li, *Polyhedron*, 2012, **33**, 273–279.
18 P. Ma, F. Hu, Y. Huo, D. Zhang, C. Zhang, J. Niu and J. Wang, *Cryst. Growth Des.*, 2017, **17**, 1947–1956.
19 G. A. Bain and J. F. Berry, *J. Chem. Educ.*, 2008, **85**, 532–536.
20 D. N. Woodruff, R. E. P. Winpenny and R. A. Layfield, *Chem. Rev.*, 2013, **113**, 5110–5148.
21 S. Cardona-Serra, J. M. Clemente-Juan, E. Coronado, A. Gaita-Ariño, A. Camoon, M. Evangelisti, F. Luis, M. J. Martinez-Perez and J. Sese, *J. Am. Chem. Soc.*, 2012, **134**, 14982–15990.
22 W. Cañon-Mancisidor, S. G. Miralles, J. J. Baldoví, G. M. Espallargas, A. Gaita-Ariño and E. Coronado, *Inorg. Chem.*, 2018, **57**, 14170–14177.
23 J. J. Baldoví, E. Coronado, A. Gaita-Ariño, C. Gamer, M. Giménez-Marqués and G. Mínguez Espallargas, *Chem. - A Eur. J.*, 2014, **20**, 10695–10702.
24 N. Ishikawa, M. Sugita and W. Wernsdorfer, *J. Am. Chem. Soc.*, 2005, **127**, 3650–3651.
25 J. Ruiz, A. J. Mota, A. Rodríguez-Diéguez, S. Titos, J. M. Herrera, E. Ruiz, E. Cremades, J. P. Costes and E. Colacio, *Chem. Commun.*, 2012, **48**, 7916–7918.
26 V. E. Campbell, R. Guillot, E. Riviere, P.-T. Brun, W. Wernsdorfer and T. Mallah, *Inorg. Chem.*, 2013, **52**, 5194–5200.
27 N. Ishikawa, M. Sugita, T. Ishikawa, S. Y. Koshihara and Y. Kaizu, *J. Am. Chem. Soc.*, 2003, **125**, 8694–8695.
28 G.-J. Chen, C.-Y. Gao, J.-L. Tian, J. Tang, W. Gu, X. Liu, S.-P. Yan, D.-Z. Liao and P. Cheng, *Dalt. Trans.*, 2011, **40**, 5579.
29 R. Orbach, *Proc. R. Soc. A Math. Phys. Eng. Sci.*, 1961, **264**, 458–484.
30 J. Tang and P. Zhang, *Lanthanide Single Molecule Magnets*, Springer Berlin Heidelberg, Berlin, Heidelberg, 2015.
31 J. Ruiz, G. Lorusso, M. Evangelisti, E. K. Brechin, S. J. A. Pope and E. Colacio, *Inorg. Chem.*, 2014, **53**, 3586–3594.
32 Y. Rechkemmer, J. E. Fischer, R. Marx, M. Dörfel, P. Neugebauer, S. Horvath, M. Gysler, T. Brock-Nannestad, W. Frey, M. F. Reid and J. van Slageren, *J. Am. Chem. Soc.*, 2015, **137**, 13114–13120.
33 S.-S. Liu, L. Xu, S.-D. Jiang, Y.-Q. Zhang, Y.-S. Meng, Z. Wang, B.-W. Wang, W.-X. Zhang, Z. Xi and S. Gao, *Inorg. Chem.*, 2015, **54**, 5162–5168.
34 M. Gregson, N. F. Chilton, A.-M. Ariciu, F. Tuna, I. F. Crowe, W. Lewis, A. J. Blake, D. Collison, E. J. L. McInnes, R. E. P. Winpenny and S. T. Liddle, *Chem. Sci.*, 2016, **7**, 155–165.
35 K. S. Pedersen, L. Ungur, M. Sigrist, A. Sundt, M. Schau-Magnussen, V. Vieru, H. Mutka, S. Rols, H. Weihe, O. Waldmann, L. F. Chibotaru, J. Bendix and J. Dreiser, *Chem. Sci.*, 2014, **5**, 1650–1660.
36 T. T. Cunha, J. Jung, M. Boulon, G. Campo, F. Pointillart, C. L. M. Pereira, B. Le Guennic, O. Cador, K. Bernot, F. Pineider, S. Golhen and L. Ouahab, *J. Am. Chem. Soc.*, 2013, **135**, 16332–16335.
37 Q.-W. Li, J.-L. Liu, J.-H. Jia, J.-D. Leng, W.-Q. Lin, Y.-C. Chen and M.-L. Tong, *Dalt. Trans.*, 2013, **42**, 11262.
38 L.-F. Wang, J.-Z. Qiu, J.-L. Liu, Y.-C. Chen, J.-H. Jia, J. Jover, E. Ruiz and M.-L. Tong, *Chem. Commun.*, 2015, **51**, 15358–15361.
39 E. Lucaccini, L. Sorace, M. Perfetti, J.-P. Costes and R. Sessoli, *Chem. Commun.*, 2014, **50**, 1648–1651.
40 C. Dekker, A. Arts, H. de Wijn, A. van Duyneveldt and J. Mydosh, *Phys. Rev. Lett.*, 1988, **61**, 1780–

1783.
41 L. Chen, J. Zhou, A. Yuan and Y. Song, *Dalt. Trans.*, 2017, **46**, 15812–15818.
42 J. J. Le Roy, L. Ungur, I. Korobkov, L. F. Chibotaru and M. Murugesu, *J. Am. Chem. Soc.*, 2014, **136**, 8003–8010.
43 I. F. Díaz-Ortega, J. M. Herrera, T. Gupta, G. Rajaraman, H. Nojiri and E. Colacio, *Inorg. Chem.*, 2017, **56**, 5594–5610.
44 J. Dreiser, *J. Phys. Condens. Matter*, 2015, **27**, 183203.
45 A. Adhikary, J. A. Sheikh, S. Biswas and S. Konar, *Dalt. Trans.*, 2014, **43**, 9334–9343.
46 J. Bartolomé, G. Filoti, V. Kuncser, G. Schinteie, V. Mereacre, C. E. Anson, a. K. Powell, D. Prodius and C. Turta, *Phys. Rev. B - Condens. Matter Mater. Phys.*, 2009, **80**, 1–16.
47 F. Luis, J. Bartolomé, J. F. Fernández, J. Tejada, J. M. Hernández, X. X. Zhang and R. Ziolo, *Phys. Rev. B*, 1997, **55**, 11448–11456.